Atmos. Chem. Phys. Discuss., 11, 21055–21090, 2011
www.atmos-chem-phys-discuss.net/11/21055/2011/
doi:10.5194/acpd-11-21055-2011

Atmospheric Chemistry and Physics Discussions

The sensitivity of secondary organic aerosol (SOA) component partitioning to the predictions of component properties – Part 3: Investigation of condensed compounds generated by a near-explicit model of VOC oxidation

M. H. Barley, D. Topping, D. Lowe, S. Utembe, and G. McFiggans

Centre for Atmospheric Sciences, School of Earth Atmospheric & Environmental Sciences, University of Manchester, Manchester, M13 9PL, UK

Received: 1 June 2011 – Accepted: 15 July 2011 – Published: 27 July 2011

Correspondence to: G. McFiggans (g.mcfiggans@manchester.ac.uk)

Published by Copernicus Publications on behalf of the European Geosciences Union.

Abstract

Calculations of the absorptive partitioning of secondary organic aerosol components were carried out using a number of methods to estimate vapour pressure and non-ideality. The sensitivity of predicted condensed component masses, volatility, O:C ratio, molar mass and functionality distribution to the choice of estimation methods was investigated in mixtures of around 2700 compounds generated by a near explicit mechanism of atmospheric VOC degradation. The sensitivities in terms of all metrics were comparable to those previously reported (using 10 000 semi-randomly generated compounds). In addition, the change in predicted aerosol properties and composition with changing VOC emission scenario was investigated showing key dependencies on relative anthropogenic and biogenic contributions. Finally, the contribution of non-ideality to the changing distribution of condensed components was explored in terms of the shift in effective volatility by virtue of component activity coefficients, clearly demonstrating both enhancement and reduction of component masses associated with negative and positive deviations from ideality.

1 Introduction

Gas to particle mass transfer of semi-volatile components, and the production of secondary organic material (SOA), is an important factor in determining the evolving chemical composition of aerosol particles. A representation of the mass transfer, or at least of the equilibrium partitioning between the phases, is necessary for predicting their loading and composition. Even a basic identification of organic compounds in particulate matter is incomplete and a full component mass balance has never been achieved (Hallquist et al., 2009; Hamilton et al., 2008). To attempt prediction of condensable gas phase components, it is possible to make use of mechanistic models that track the oxidation of atmospheric volatile organic compounds (VOCs) all the way through to carbon dioxide and water. Such a mechanism is the Master Chemical Mechanism (MCM) describing the degradation of about 100 VOCs (Jenkin et al., 1997, 2003; Saunders et al., 2003; Bloss et al., 2005).

ACPD
11, 21055–21090, 2011

In Part 1 of this series (McFiggans et al., 2010) the sensitivity of key SOA properties (condensed SOA mass, O:C ratio, molar mass, volatility and functionality distributions) to the choice of vapour pressure (p^0) and non-ideality (γ_i) prediction methods used in the partitioning calculations was systematically investigated. The role of SOA complexity in this sensitivity study was also studied by using multiple mixtures of 2, 10, 100, 1000 or 10 000 randomly generated molecules. The results showed that the condensed SOA mass was highly sensitive to the vapour pressure model and much less sensitive to the activity coefficient model and the number of components used to represent the model. In Part 2 of this series (Topping et al., 2011) the methods developed in Part 1 were applied to determine the sensitivity of key SOA particle properties (density, hygroscopicity, and cloud condensation nuclei activation potential) to the models used for p^0 and γ_i and the chemical complexity of the SOA. The results showed that, providing only water evaporated when drying, predicted hygroscopic growth factors were relatively insensitive to the choice of p^0 model but more sensitive to the inclusion of non-ideality. If the semi-volatile components were assumed to equilibrate on drying the aerosol particle, the sensitivity massively increased and resulted in calculated hygroscopic growth factors more typical of those measured for common inorganic salts than for atmospheric organic material. In the present paper similar calculations to those developed in Part 1 are done, but instead of using randomly generated compounds the calculations were applied to 2742 atmospherically relevant molecules obtained from the output of the MCM. The sensitivity of the same key SOA properties to p^0 model and non-ideality were assessed for comparison with the results of Part 1 but with components and concentrations provided by simulations of oxidative degradation of VOCs. No comparisons to the results in Topping et al. (2011) are made (such comparisons may be a topic for further work). In addition the present paper also explores the predicted properties of SOA formed over a wide range of emission scenarios (by varying inputs of anthropogenic and biogenic VOCs and NO_x), and the distribution and range of activity coefficients to be found in condensed aerosol.

ACPD
11, 21055–21090, 2011

2 Methodology

In McFiggans et al. (2010) sensitivities were calculated using molecular structures based upon randomly combined UNIFAC groups (Fredenslund et al., 1975) subdivided (where appropriate) to provide the groups required for the physical property estimation methods. Atmospheric concentrations were calculated from the number of carbon atoms in a structure after scaling so that the base case model gave 10.0 $\mu g\,m^{-3}$ SOA under standard conditions. These inputs (p^0, γ_i (when required), total concentrations of all organic species, temperature and relative humidity) were used in the partitioning model (see Eqs. (1–3) in McFiggans et al., 2010) to determine the condensed mass and composition, from which the other properties, defined above, can be derived. In the present work the input molecular structures are provided by the MCM closed shell oxidation products along with their atmospheric concentrations (changing with scenario).

Vapour pressures (p^0) of all closed-shell (non-radical) compounds formed from VOC degradation by the MCM were predicted using a number of methods. Single time-slices of compound concentrations were extracted from predictions under a range of emission scenarios (described below). Using these as input to the partitioning approach described by Barley et al. (2009) with each of the p^0 techniques described in McFiggans et al. (2010) (and γ_i calculated from UNIFAC when exploring non-ideality) the fraction of each component in the condensed phase was calculated, along with the distributions of O:C ratio, molar mass and functional groups.

2.1 Model scenarios and conditions

MCM simulations representing a wide range of emission scenarios from UK industrial/urban (high anthropogenic and low biogenic inputs) through to rural background conditions (higher biogenic and low anthropogenic inputs) were conducted. Emissions representing average UK National Atmospheric Emissions Inventory (NAEI) totals for the year 2001 (3740 ktonnes CO, 1130 ktonnes SO_2, 1680 ktonnes NO_x, and 1510 ktonnes speciated VOCs with 1330 ktonnes being anthropogenic (AVOCs) were

ACPD
11, 21055–21090, 2011

continuously emitted into the box throughout the base case model run. The snapshots were taken at 18:00 h on the 13th day after the beginning of the simulation. A fairly constant diurnal profile in simulated ozone and degradation intermediates was simulated after 9 model days and conditions at 18:00 h represent the late afternoon peak in photochemistry. Similar sensitivities might be reasonably expected from alternative time slices, but this is outside the scope of the present work and could form the subject of further analyses. Further emission scenarios were simulated by independently multiplying the AVOCs, biogenic VOCs (BVOCs) and NO_x component of the base case emissions by factors of 0.01, 0.1, 10, 100 and 1000 to give 206 emission scenarios covering a range of 6 orders of magnitude in the emitted concentrations. To study the trends in predicted aerosol properties and composition with emission levels (see Sect. 3 below), the full range of scenarios was used. For the studies on the sensitivity of SOA properties to the p^0 and γ_i models used (see Sect. 4 below) partitioning calculations were limited to the 27 scenarios in which the multiplying factors were restricted to 0.1,1.0 and 10 to ensure that the more atmospherically relevant scenarios were used. For those calculations using a single scenario, the 1.0/1.0/1.0 NO_x/AVOC/BVOC scenario was selected, as it was taken to best represent average UK emissions, and will be referred to as the standard scenario when used in the examples below.

The limitations of such an average UK emissions scenario should be recognised. The complexity of the chemical system lends itself to box model simulations with inherent structural assumptions and simplifications in their input conditions. One of the assumptions introduced in the current study is uniformity of pollutant concentration across each simulation by virtue of the UK averaged emissions, representing the UK boundary layer atmosphere as one well mixed box. Consequently, whilst a wide range of emission scenarios are used in order to investigate a broad range of chemical space relative to the base case scenario of 2001 UK emission totals, no single scenario can be claimed to be completely representative of any real single location.

ACPD
11, 21055–21090, 2011

For each emission scenario the partitioning calculation was conducted at a number of temperature, RH and involatile core mass values requiring in total 32 sets of calculations for each emission scenario using around 2700 compounds (see Table 1). The temperature and RH values were selected to cover the range of typical conditions found in a temperate maritime climate such as that of the UK. The core is assumed to interact ideally with all components and is assigned a molar mass of 320 g mole^{-1}, representing low volatility oxygenated background material, based on the analysis of water soluble organic compounds (WSOC) reported by Reemtsma et al. (2006).

2.2 The estimation of physical properties using group contribution methods

The selection of vapour pressure (p^0) estimation methods has already been described by McFiggans et al. (2010) and we continue to use the same nomenclature in this work. The boiling point (T_b) estimation methods of Nannoolal et al. (2004); Stein and Brown (1994), and Joback and Reid (1987) will henceforth be referred to as the N, SB and JR methods respectively. The p^0 equations used in this work are those of Nannoolal et al. (2008) and of Myrdal and Yalkowsky (1997); referred to as the N/VP and MY methods respectively. Hence there are six different methods for estimating p^0 considered in this work (as in McFiggans et al., 2010 and Topping et al., 2011) of which the N-N/VP method is used as the base case. The other combinations compared to the base case when investigating the sensitivity of SOA properties to p^0 estimation method are SB-N/VP, JR-N/VP, N-MY, SB-MY, and JR-MY (see Table 2). For more details about the p^0 estimation methods see McFiggans et al. (2010) and Barley and McFiggans (2010). Parameters for atmospherically important functional groups (e.g. hydroperoxide, peroxyacid, nitrate and PAN) that are not covered by the original methods were either obtained from the literature (e.g. Compernolle et al., 2010; Camredon and Aumont, 2006); or the unknown groups were further divided into smaller groups that were recognised by the estimation method.

Activity coefficients were calculated using original UNIFAC (Fredenslund et al., 1975) with group parameters obtained from Hansen et al. (1991), and using the updated

ACPD
11, 21055–21090, 2011

parameters (for OH and COOH subgroups) of Peng et al. (2001). More complex groups not covered by UNIFAC were converted into recognised subsidiary groups with the priority being to account for all the heavy atoms (e.g. nitrate = nitro plus ether; carbonate = ester plus ether).

A significant proportion (22 %) of the non-ideal calculations suffered from problems with convergence. These were found to be concentrated at the highest and lowest RH values. For the purpose of this study, all non-ideal calculations which presented convergence problems were excluded. For the standard scenario 7 of the 32 cases failed to converge correctly. There is no indication that these non-converging cases are systematically biased towards either positive or negative deviations from ideality.

For convenience, when calculating the properties of large numbers of component molecules using the relatively complex estimation methods, their fragmentation into contributing groups was automated. The automated parsing and fragmentation methods is described in more detail (with some examples) in the Supplement. Whilst they can in principle be used with the output of any model, the fragmentation methods used here have been tailored to the output of the MCM.

2.3 The gas/liquid partitioning model

The mole based partitioning model has been described in detail elsewhere (e.g. Sect. 2.1 in Barley and McFiggans, 2010; Barley et al., 2009), and yields identical results to the conventional mass based model of Pankow (1994).

The partitioning constant $K_{p,i}$, in units of $m^3 \mu mol^{-1}$ is given by Eq. (1)

$$K_{p,i} = \frac{C_i^{cond}}{C_i^{vap} C_{OA}} = \frac{RT\ f}{10^6 \gamma_i p_i^0} \quad (1)$$

where

C_i^{vap} is the vapour phase molar concentration of component i, $\mu mol\, m^{-3}$,

C_i^{cond} is the condensed phase molar concentration of component i, $\mu mol\, m^{-3}$,

ACPD
11, 21055–21090, 2011

C_{OA} is the total molar concentration of condensed organic material, μmol m^{-3},
p_i^0 is the saturated vapour pressure of component i, atm,
R is the ideal gas constant = 8.2057 × 10^{-5} m^3 atm mol^{-1} K^{-1},
T is the temperature, K
f is the fraction of the condensed material that may be considered absorptive, usually considered unity for most absorptive partitioning calculations and
γ_i is the activity coefficient for component i in the liquid phase.
Defining a partitioning coefficient ξ_i for compound i given its $K_{p,i}$ value:

$$\xi_i = \left(1 + \frac{1}{K_{p,i} C_{OA}}\right)^{-1} \quad (2)$$

where the total molar concentration of condensed organic material, C_{OA}, is given by the sum of the products of the individual total component concentrations in both phases and their partitioning coefficient:

$$C_{OA} = \sum_i C_i \xi_i \quad (3)$$

where $C_i = C_i^{vap} + C_i^{cond}$ is the total loading of component i, μmol m^{-3}.

As described by McFiggans et al. (2010) the "base case" for the sensitivity studies is defined as the N-N/VP method with liquid phase ideality; but now using the 2742 MCM compounds (2727 in the special case described below).

2.4 Special case: hydrolysis of acid anhydrides

In these simulations, it is assumed that condensation to form aerosol occurs in the moist lower troposphere. Given sufficient time, it might be expected that the complex functionality available to react in the condensed phase would lead to different composition than that predicted assuming attainment of unreactive equilibrium. Owing to

ACPD
11, 21055–21090, 2011

the high water vapour mixing ratio and the predicted and measured concentration of water in ambient aerosol, it is probable that some water will lead to hydration of certain hydrophilic molecules and relatively rapid hydrolysis of acid anhydrides. Acids are more polar than anhydrides and are expected to have lower vapour pressures. For example, the conversion of maleic anhydride and methyl maleic anhydride to the corresponding diacids reduce their respective vapour pressures by a factor of about 30 000. Acknowledging that it is only one of many potential classes of condensed reaction in the complex ambient aerosol matrix, all anhydrides were allowed to hydrolyse to the appropriate acid(s) and the vapour pressure of the acids was used to partition these species into the condensed phase: note that this assumption is equivalent to an assumption of instantaneous hydrolysis. In all, 47 acid anhydrides were identified and their hydrolysis led to the loss of 15 compounds from the original list of MCM compounds (from 2742 down to 2727). It should be noted that dicarboxylic acids are a well established, if minor, component of SOA (Bilde et al., 2003; Hallquist et al., 2009), but with the exception of pinic and norpinic acid are absent from the output of the MCM. The MCM does predict significant concentrations of cyclic anhydrides, especially for anthropogenically dominated scenarios, and their hydrolysis to the corresponding dicarboxylic acids both increases SOA amounts and provides a higher proportion of carboxylic acid groups in the predicted SOA.

For the estimation of vapour pressures of dicarboxylic acids, a correction for the Nannoolal T_b was included (see Supplement for derivation) to correct a systematic error for this class of compounds.

$$\Delta T = -9.2169C + 84.11 \quad (4)$$

where C is the number of carbon atoms in the diacid. This correction is about +50 K for a C4 diacid, +20 K for a C7 and becomes negative for a C10 molecule (it is <2 K for Pinic acid). It should not be used outside the range C3–C12.

ACPD
11, 21055–21090, 2011

3 Results and discussion: dependence of the properties of the condensed material on emission scenario

Figures 1, S1 and S2 (see Supplement) show predicted particulate properties across a range of emissions. These plots are analogous to the conventional isopleths used to illustrate the dependence of ozone production on VOC and NO_x. The properties are logarithm of the average condensed mass ($\mu g\,m^{-3}$); average O:C ratio; molar mass and average N:C ratio. When plotting ozone isopleths, it is important that the "specific reactivity" of the VOC mixture is constant with increasing VOC. It is not clear that an analogous "specific particulate forming capacity" of a mixture exists that should be maintained constant in the current plots. Figure 1 shows the variability in the properties when simultaneously increasing the AVOC and BVOC emissions at equal rates. Figure S1 in the Supplement shows variability in the properties for the 35 scenarios with the lowest biogenic input (0.01); S2 shows them for the 35 scenarios with the lowest anthropogenic input (also 0.01). All averages were calculated for the same atmospherically relevant case within a scenario $T = 293.15\,K$, % RH = 70 and $3.0\,\mu g\,m^{-3}$ involatile core. All three figures show similar trends with rising VOC and NO_x, suggesting a minimal dependence on the AVOC:BVOC ratio: i.e. a unit of AVOC is as likely to create SOA as a unit of BVOC. In contrast to conventional ozone isopleths, the SOA mass increases with increasing VOC, but has a more complex NO_x-dependence, showing a maximum at intermediate NO_x levels (see Fig. 1). As the VOC levels decrease, the presence of NO_x appears inhibitory to SOA formation. The O:C ratio appears to follow a trend more analogous to classical ozone isopleth, showing an increase with increasing VOC and NO_x, but falling off in both VOC- and NO_x-limited regions. A similar trend is shown for N:C ratio, though showing less NO_x limitation than VOC limitation. The average molar mass shows a more complex picture, increasing with lower VOC emissions and generally with increasing NO_x. The total condensed SOA mass shows a greater variation with emissions than the other properties; varying over 7 or 8 orders of magnitude.

ACPD
11, 21055–21090, 2011

4 Results and discussion: sensitivity of SOA properties to estimated vapour pressures and activity coefficients

Figure 2 shows the sensitivity of condensed SOA mass to the methods used to estimate vapour pressure and the treatment of solution ideality across all conditions for 27 model scenarios. This figure is directly comparable to Figs. 3 and 4 in McFiggans et al. (2010). The base case uses the p^0 method N-N/VP with all γ_i set to unity (ideal case). In the first five boxes of Fig. 2 the liquid phase is assumed to be ideal but the p^0 method is changed and the factor by which the condensed mass changes is plotted. In the sixth box the p^0 method is N-N/VP, liquid phase ideality is still assumed but all the acid anhydrides are hydrolysed . In the seventh box the vapour pressure used is still N-N/VP but the γ_i of all components are calculated by UNIFAC. Comparison of the first six bars with the final bar demonstrates that the condensed mass can change by several orders of magnitude for some cases with a change in p^0 estimation method but the effect of including non-ideality is much less significant (very few cases show a mass less than a tenth of the base case). These results confirm the significant conclusions drawn from Figs. 3 and 4 in McFiggans et al. (2010) and are similarly in contrast with the finding that non-ideality is a greater contributor to the variability in particle hygroscopicity as shown by Topping et al. (2011). The plots are also consistent with the conclusions about the vapour pressure estimation methods reported in Barley and McFiggans (2010): the SB and N methods for T_b estimation give similar results while the JR method significantly overestimated T_b. Hence in Fig. 2 the SB-N/VP method shows the smallest interquartile range (size of the box in the box-whisker plot) of any of the vapour pressure methods while the two Joback methods (JR-N/VP and JR-MY) show a significant bias towards increased mass. Also, the methods using the MY vapour pressure method generate less SOA mass than the corresponding methods using the N/VP method (in some cases by some orders of magnitude) and this has been explained by the MY vapour pressure equation underestimating the slope of the vapour pressure curve (Barley and McFiggans, 2010). Some statistics for the scatter

ACPD
11, 21055–21090, 2011

depicted in this figure are summarised in Table 3 and confirm that the non-ideal model shows less deviation from the base case than all the p^0 models except SB-N/VP. Note that the hydrolysis of anhydrides can substantially increase the amount of SOA mass (several cases show an increase of between 10 and 100 times) and this is associated with a combination of high levels of NO_x and AVOC combined with low levels of BVOC, so it may be expected that some of the measured dicarboxylic acids in the ambient atmosphere under moist polluted conditions may be attributable to the hydrolysis of anhydrides.

4.1 SOA composition

Here we briefly assess the impact of the predictive technique on the SOA composition; specifically the order of compound contribution to SOA. The chemical composition of the SOA is very sensitive to the vapour pressure model used and the inclusion of non-ideality. In Fig. 3 this is shown by the change in position of the top 200 compounds with respect to the order using the base case method at 293 K and 70 % RH for the standard scenario. The methodology is taken from Valorso et al. (2011) where the authors describe SOA formation using a much more detailed oxidation mechanism than the MCM (GECKO-A see Aumont et al., 2005; Camredon et al., 2007) but degrading only one VOC (α-pinene) and demonstrate the change in SOA composition with vapour pressure model using similar figures. Figure 3 confirms that all the models, except the special case involving hydrolysis of acid anhydrides, cause a substantial reordering of the compounds. Figure S3 in the Supplement shows similar results for both a low temperature/high % RH case, and a high temperature/low % RH case using the standard scenario confirming that the results seen in Fig. 3 are typical. It is not surprising that hydrolysis of anhydrides does not greatly change the compound ordering as the vast majority of compounds have the same vapour pressure as they have in the base case calculation. The hydrolysis of anhydrides changes the vapour pressure of some 32 compounds (out of 2727) and substantially increases the SOA mass which does affect the relative contributions of the other components but the effect is small compared with

ACPD
11, 21055–21090, 2011

the effects upon the order due to changing the p^0 or γ_i models. Potentially of greatest interest is that the largest re-ordering of the most important contributing compounds results from the inclusion of non-ideality. Given the relatively low variation in mass attributable to the inclusion of non-ideality, it is evident that the reordering must be the result of simultaneous positive and negative deviations from ideality in the multicomponent mixture. Figure S3 in the Supplement shows that this is further exaggerated under cooler, moister conditions and only slightly less important under warm dry conditions.

4.2 Volatility distributions

Figure 4 shows the volatility distribution of the 2742 MCM compounds using the standard scenario (1.0/1.0/1.0 for NO_x/AVOC/BVOC) at atmospherically relevant conditions ($T = 293.15$ K, % RH = 70, core = 3.0 µg m^{-3}). This case was selected simply for illustration, representing simulations under average UK emission conditions with temperature and RH selected to represent conditions in the lower Troposphere, while ensuring that the appropriate non-ideal calculations converged correctly. It should be noted that under these conditions, the amount of SOA predicted (about 0.055 µg m^{-3} for the base case) is substantially below both the 10 µg m^{-3} condensed mass loading used as the reference case in McFiggans et al. (2010); and the amount of SOA typically found in the lower Troposphere. For example reported SOA amounts found during the TORCH campaign ranged from 0.92 to 5.91 µg m^{-3} (Johnson et al., 2006); while Heald et al. (2005) reported average organic carbon aerosol concentrations of 4 µg m^{-3} during the ACE-Asia study.

The components are binned according to their C_i^* value where this parameter is the inverse of $K_{p,i}$ as defined by Eq. (1) in McFiggans et al. (2010). As found in this earlier paper, the volatility distributions show substantial sensitivity to the vapour pressure model used with components moving between the logC_i^* bins. The tendency for the JR method to overestimate T_b, leading to reduced vapour pressures, causes the bunching of compounds into the lower volatility bins (log$C_i^* < -2$). If the hydrolysed case is

ACPD
11, 21055–21090, 2011

compared to the base case then it is clear that the hydrolysis process reduces the concentration in bin $\log C_i^* = +2$ and possibly some further bins of even higher volatility, while significantly increasing the amount of material in bin $\log C_i^* = -2$. This is due to the hydrolysis of some highly abundant cyclic anhydrides to give much less volatile dicarboxylic acids which then appear in the $\log C_i^* = -2$ bin. The effect of the inclusion of non-ideality in the partitioning calculation changes the volatility distribution much less than the two T_b by JR p^0 methods, but by more than some of the other methods (note that $\log C_i^*$ values for the non-ideal case do not include the activity coefficients and represent the saturation concentrations of the components under ideal conditions). In general these figures show that the assignment of compounds to a volatility bin is extremely sensitive to the p^0 and γ_i models used. Hence the least volatile compounds (a series of multifunctionalised cyclohexenes) as determined by the N-N/VP method are in bin $C_i^* < -5$ using this method, as they are for the SB-N/VP, hydrolysed, and non-ideal models. For the N-MY model they appear in the $\log C_i^* = -3$ bin and for the SB-MY model they are in the $\log C_i^* = -4$ bin. Given this sensitivity to the p^0 model the idea that lumping species together by assigning molecules to volatility bins on the basis of vapour pressure and being able to make meaningful predictions of their properties seems highly optimistic.

4.3 O:C ratio and molar mass distributions

The two panels in Fig. 5 show the concentration of the condensed compounds binned according to their molar mass and O:C ratio for two vapour pressure models (N-N/VP (base case) and JR-N/VP) corresponding to the first and third panels on the top row of Fig. 4 for the "standard" 1.0/1.0/1.0 emission scenario under the same conditions as Fig. 4. The colour axis is the base 10 logarithm of the cumulative concentration in the respective bin, with the bin size being defined as 0.25 units of O:C ratio by 20 amu. As expected, more condensed material is predicted when the JR estimation method is used for T_b. Figure 6 shows the ratio of the binned condensed phase loading using the two vapour pressure methods. The similarity in the shape of the three figures

ACPD
11, 21055–21090, 2011

suggests a consistent under-prediction of volatility for each O:C ratio and molar mass bin when using the JR estimation method. If the right hand side of Fig. 6 (molar mass above 200 amu) is compared to the corresponding figure (Fig. 9c) in McFiggans et al. (2010) substantial similarities can be seen confirming that differences in predicted SOA composition with vapour pressure estimation techniques are not completely systematic and independent of functionality. Comparing the position of the concentration peaks in Figs. 5 and 6 (despite the broadness of the features) it is clear that the peak in Fig. 6 is at a substantially lower molar mass than the peaks in Fig. 5. This clearly demonstrates that the extra material condensing when using the JR-N/VP p^0 model has, on average, a lower molar mass than the material condensing using the N-N/VP model. There may also be changes in the O:C ratio but this is not as clear as the change in molar mass in these figures. This confirms (as stated in McFiggans et al., 2010) that the choice of estimation methods used in absorptive partitioning calculations will substantially impact upon the selection of semivolatile components and hence the properties (such as O:C ratio and average molar mass) of the organic fraction of the condensed phase.

Figure 7 is directly comparable to Fig. 10 in McFiggans et al. (2010) showing the difference and variability in the average O:C ratio and molar masses of the predicted condensed mass. The black asterisk (no associated box-whisker plots) shows the median O:C ratio and molar mass for the base case; the black triangle shows these parameters for the non-ideal case; and the black circle shows these parameters for the case with hydrolysis. The remaining coloured symbols are associated with the box-whisker plots and show the variation of these parameters with vapour pressure method.

As expected this plot has a similar form to Fig. 10 in McFiggans et al. (2010), with a similar clustering of the median values. The main difference being the outlier at low molar mass due to the hydrolysed case (no equivalent case is shown in Fig. 10 of McFiggans et al., 2010), and that the median values are at higher O:C ratio (0.76 compared to 0.39 for the base case), and slightly lower molar mass (214 vs. 270) than the equivalent values in the Part 1 figure. The calculated O:C ratio of 0.76 for the base

ACPD
11, 21055–21090, 2011

case is substantially higher than the O:C ratio reported in recent studies of atmospheric aerosol in heavily urbanised areas: generally below 0.5 in London (Allan et al., 2010), and 0.36 in the New York area (Sun et al., 2011); but similar to the value of up to 0.8 for aged aerosol measured in the outflow from Mexico city (DeCarlo et al., 2008).

For molar mass the median values of 214 (or 155 for the hydrolysed case) will be substantially below an average value measured for an atmospheric sample due to the formation of oligomers (Reinhardt et al., 2007; Reemtsma et al., 2006) which are not considered in our model.

In Fig. 7 the differences between the base case and the hydrolysed case result from the maleic acid derivatives in the hydrolysed case as these have lower molar mass and higher O:C ratio than the average of the condensed components. It is clear from the box-whisker plots that the spread in O:C ratio and molar mass values is much smaller for the two methods that use T_b by JR. The increase in condensed mass associated with this boiling point method also leads to a lower median O:C ratio and molar mass-consistent with higher volatility components with a lower O:C ratio and lower molar mass becoming included in the SOA mass.

4.4 Average functionality

The most abundant functional groups in the predicted SOA were alcohols, hydroperoxides and ketones. In a recent publication (Valorso et al., 2011) the authors found the same three functional groups dominating predicted SOA composition for a low NO_x scenario; although hydroperoxides were more prevalent than alcohols. Figure 8 shows the sensitivity of the average number of functional groups per molecule for these top three functional groups to changes in vapour pressure values, the inclusion of non-ideality, and the effect of hydrolysing the acid anhydrides. In general the distribution of the number of functional groups is relatively insensitive to the vapour pressure method used. This is particularly true for the hydroperoxides and ketones; less true for alcohols. For alcohols the striking feature is that some cases give predicted SOA with an average of more than 2.5 alcohols per molecule. It is noticeable that the JR-N/VP and

ACPD
11, 21055–21090, 2011

JR-MY methods (that predict much more SOA mass- see Fig. 2) do not show these extreme levels of alcohol participation suggesting that the high alcohol levels may be associated with very low SOA mass. At very low SOA mass the polyalcohols are important contributors to SOA mass giving high O:C ratios and high average molar mass. When more mass is condensed the polyalcohols become less important as components with lower molar mass and O:C ratio are included in the condensed material. This is consistent with the lower O:C ratios and lower median molar mass seen for the p^0 methods using T_b by JR in Fig. 7.

For the case including hydrolysis of anhydrides the average composition of SOA across 27 scenarios was significantly different to the base case with carboxylic acids displacing ketones to become the third most abundant functional group. This change is almost certainly due to the preponderance of maleic acid derivatives in the anthropogenically dominated scenarios after hydrolysis. This increase in carboxylic acid groups leads to a substantial reduction in the number of alcohols, hydroperoxides and ketones for the hydrolysed case (see Fig. 8). Note that the non-ideal case shows a very similar distribution for these top three functional groups to the base case.

The fourth and fifth most important functional groups in the predicted SOA are nitrate and nitro. The relatively high abundance of these groups is reflected in the high median N:C ratio (0.1212), which is also significantly higher than the recently reported (Sun et al., 2011) value for urban aerosol (0.012).

4.5 Variation in component non-ideality

Figure 9 illustrates the variation in component non-ideality, for all the MCM components, for the standard scenario at 293 K and a range of RH values. This is represented by the variation in the logarithm of the predicted component activity coefficients with O:C ratio and saturation concentration. It is clear that there is a wide variation in component activity coefficient, particularly at high % RH, ranging over several orders of magnitude (from 0.001–0.01 for some components in the bin $\log C_i^* = -4$, up to 10^5 for components in $\log C_i^* = +4$). The lowest activity coefficients are associated with the

ACPD
11, 21055–21090, 2011

lowest volatility bins so these compounds (including the multifunctionalized cyclohexenes mentioned in Sect. 4.2) may dominate SOA composition at low SOA mass. In contrast the highest activity coefficients are associated with high volatility bins meaning that they are unlikely to contribute to SOA. These results demonstrate that the MCM compounds exhibit both salting in (activity coefficients below unity) and salting out (greater than unity) at all relative humidities. It should be noted that, whilst it may be expected that components with high activity coefficients would tend to separate into one or more additional phases, those with low activity coefficients are very stable in the predicted mixture. It is therefore necessary to consider both positive and negative deviations from ideality to capture the effect of non-ideality on absorptive partitioning. In Donahue et al. (2011) the authors develop a two-dimensional volatility basis set model which allows the prediction of γ_i from the volatility and O:C ratio of a component (see their Fig. 9). This model specifically aims to address salting out in POA/SOA mixtures and does not consider components to have $\gamma_i < 1$. From Fig. 9 (and the component reordering exhibited in Fig. 3), it is clear that it is necessary to consider whether both positive and negative deviations from ideality will play a role in systems of interest in the atmosphere. The AIOMFAC model of Zuend et al. (2011) allows explicit consideration of phase separation in mixtures of inorganic and organic components and efforts are underway to explicitly include this consideration in the sensitivity studies. This will form the basis for subsequent publications.

5 Conclusions

Calculations of the absorptive partitioning of secondary organic aerosol components were carried out using a number of methods to estimate vapour pressure and non-ideality. The sensitivity of predicted condensed component masses, volatility, O:C ratio, molar mass and functionality distribution to the choice of estimation methods was investigated in mixtures of around 2700 compounds generated by a near explicit mechanism of atmospheric VOC degradation. In a previous publication, the same sensitivity

ACPD
11, 21055–21090, 2011

study was carried out for semi-randomly generated compounds, with the number of compounds ranging from 2 to 10 000. The two sets of compounds used in that study and in this report do have significant features in common. The condensed material from both sets are dominated by multifunctional compounds with a high proportion of oxygenated functionality which tend to give low or very low vapour pressures. The MCM compounds show a greater diversity of the carbon skeleton supporting the functional groups, although the effect of this should be minimal as the calculations of p^0 and γ_i are largely driven by the functional groups .

In summary the results presented here agree with the main conclusion of McFiggans et al. (2010); namely that the variability from the base case attributable to non-ideality is not so large as the variability attributable to the selection of a vapour pressure model. This work demonstrates this for condensed SOA mass, volatility distribution, functional group distribution for the top three functional groups, O:C ratio and molar mass. Properties such as O:C ratio, average molar mass and average number of functional groups per molecule show much less sensitivity to physical property inputs than SOA mass. In addition the trends in key physical properties of condensed SOA over a wide range of emission scenarios have been explored at low BVOC, low AVOC and AVOC=BVOC. The trends suggest that the dependence of the properties on the VOC and NO_x emissions are independent of the AVOC:BVOC ratio. Finally an analysis of the non-ideal behaviour of the MCM compounds over a range of relative humidities show a wide range of γ_i values including very low activity coefficients for low volatility components that may dominate SOA composition at low SOA mass. This demonstrates the importance of including the possibility of salting in ($\gamma_i < 1$) in SOA models considering non-ideality.

ACPD
11, 21055–21090, 2011

Supplementary material related to this article is available online at: http://www.atmos-chem-phys-discuss.net/11/21055/2011/acpd-11-21055-2011-supplement.pdf.

Acknowledgements. This work was carried out within the UK NERC-funded "QUantifying the Earth SysTem" (QUEST) project under the "QUest Aerosol and Atmospheric Chemistry" (QUAAC) grant number NE/C001613/1) and EU-funded "European Integrated project on Aerosol Cloud Climate and Air Quality interactions" (EUCAARI) under contract number 036833-2. DOT was supported by UK National Centre for Atmospheric Sciences (NCAS) funding. Additional support was provided by the NERC-funded "Vast Improvement" project NE/E018181/1, and grant NE/H002588/1 for the development of the informatics capability.

References

Allan, J. D., Williams, P. I., Morgan, W. T., Martin, C. L., Flynn, M. J., Lee, J., Nemitz, E., Phillips, G. J., Gallagher, M. W., and Coe, H.: Contributions from transport, solid fuel burning and cooking to primary organic aerosols in two UK cities, Atmos. Chem. Phys., 10, 647–668, doi:10.5194/acp-10-647-2010, 2010. 21070

Aumont, B., Szopa, S., and Madronich, S.: Modelling the evolution of organic carbon during its gas-phase tropospheric oxidation: development of an explicit model based on a self generating approach, Atmos. Chem. Phys., 5, 2497–2517, doi:10.5194/acp-5-2497-2005, 2005. 21066

Barley, M. H. and McFiggans, G.: The critical assessment of vapour pressure estimation methods for use in modelling the formation of atmospheric organic aerosol, Atmos. Chem. Phys., 10, 749–767, doi:10.5194/acp-10-749-2010, 2010. 21060, 21061, 21065

Barley, M., Topping, D. O., Jenkin, M. E., and McFiggans, G.: Sensitivities of the absorptive partitioning model of secondary organic aerosol formation to the inclusion of water, Atmos. Chem. Phys., 9, 2919–2932, doi:10.5194/acp-9-2919-2009, 2009. 21058, 21061

Bilde, M., Svenningsson, B., Monster, J., and Rosenorn, T.: Even-Odd Alternation of Evaporation Rates and Vapor Pressures of C3-C9 Dicarboxylic Acid Aerosols, Environ. Sci. Technol., 37, 1371–1378, 2003. 21063

ACPD

11, 21055–21090, 2011

Bloss, C., Wagner, V., Jenkin, M. E., Volkamer, R., Bloss, W. J., Lee, J. D., Heard, D. E., Wirtz, K., Martin-Reviejo, M., Rea, G., Wenger, J. C., and Pilling, M. J.: Development of a detailed chemical mechanism (MCMv3.1) for the atmospheric oxidation of aromatic hydrocarbons, Atmos. Chem. Phys., 5, 641–664, doi:10.5194/acp-5-641-2005, 2005. 21056

Camredon, M. and Aumont, B.: Assessment of vapor pressure estimation methods for secondary organic aerosol modeling, Atmos. Environ., 40, 2105–2116, doi:10.1016/j.atmosenv.2005.11.051, 2006. 21060

Camredon, M., Aumont, B., Lee-Taylor, J., and Madronich, S.: The SOA/VOC/NO_x system: an explicit model of secondary organic aerosol formation, Atmos. Chem. Phys., 7, 5599–5610, doi:10.5194/acp-7-5599-2007, 2007. 21066

Compernolle, S., Ceulemans, K., and Müller, J.-F.: Technical Note: Vapor pressure estimation methods applied to secondary organic aerosol constituents from α-pinene oxidation: an intercomparison study, Atmos. Chem. Phys., 10, 6271–6282, doi:10.5194/acp-10-6271-2010, 2010. 21060

DeCarlo, P. F., Dunlea, E. J., Kimmel, J. R., Aiken, A. C., Sueper, D., Crounse, J., Wennberg, P. O., Emmons, L., Shinozuka, Y., Clarke, A., Zhou, J., Tomlinson, J., Collins, D. R., Knapp, D., Weinheimer, A. J., Montzka, D. D., Campos, T., and Jimenez, J. L.: Fast airborne aerosol size and chemistry measurements above Mexico City and Central Mexico during the MILAGRO campaign, Atmos. Chem. Phys., 8, 4027–4048, doi:10.5194/acp-8-4027-2008, 2008. 21070

Donahue, N. M., Epstein, S. A., Pandis, S. N., and Robinson, A. L.: A two-dimensional volatility basis set: 1. organic-aerosol mixing thermodynamics, Atmos. Chem. Phys., 11, 3303–3318, doi:10.5194/acp-11-3303-2011, 2011. 21072

Fredenslund, A., Jones, R. L., and Prausnitz, J. M.: Group-Contribution Estimation of Activity Coefficients in Nonideal Liquid Mixtures, AIChE Journal, 21, 1086–1099, 1975. 21058, 21060

Hallquist, M., Wenger, J. C., Baltensperger, U., Rudich, Y., Simpson, D., Claeys, M., Dommen, J., Donahue, N. M., George, C., Goldstein, A. H., Hamilton, J. F., Herrmann, H., Hoffmann, T., Iinuma, Y., Jang, M., Jenkin, M. E., Jimenez, J. L., Kiendler-Scharr, A., Maenhaut, W., McFiggans, G., Mentel, Th. F., Monod, A., Prévôt, A. S. H., Seinfeld, J. H., Surratt, J. D., Szmigielski, R., and Wildt, J.: The formation, properties and impact of secondary organic aerosol: current and emerging issues, Atmos. Chem. Phys., 9, 5155–5236, doi:10.5194/acp-9-5155-2009, 2009. 21056, 21063

Hamilton, J. F., Lewis, A. C., Carey, T. J., and Wenger, J. C.: Characterization of polar com-

ACPD
11, 21055–21090, 2011

pounds and oligomers in secondary organic aerosol using liquid chromatography coupled to mass spectrometry, Anal. Chem., 80, 474–480, 2008. 21056
Hansen, H. K., Rasmussen, P., and Fredenslund, A.: Vapor-Liquid Equilibria by UNIFAC Group Contribution. 5. Revision and Extension, Industrial and Engineering Chemistry Research, 30, 2355–2358, 1991. 21060
Heald, C. L., Jacob, D. J., Park, R. J., Russell, L. M., Huebert, B. J., Seinfeld, J. H., Liao, H., and Weber, R. J.: A large organic aerosol source in the free troposphere missing from current models, Geophys. Res. Lett., 32, L18809, doi:10.1029/2005GL023831, 2005. 21067
Jenkin, M. E., Saunders, S. M., and Pilling, M. J.: The tropospheric degradation of volatile organic compounds: A protocol for mechanism development, Atmos. Environ., 31, 81–104, 1997. 21056
Jenkin, M. E., Saunders, S. M., Wagner, V., and Pilling, M. J.: Protocol for the development of the Master Chemical Mechanism, MCM v3 (Part B): tropospheric degradation of aromatic volatile organic compounds, Atmos. Chem. Phys., 3, 181–193, doi:10.5194/acp-3-181-2003, 2003. 21056
Joback, K. and Reid, R.: Estimation of Pure-Component Properties From Group-Contributions, Chemical Engineering Communications, 57, 233–243, doi:10.1080/00986448708960487, 1987. 21060
Johnson, D., Utembe, S. R., Jenkin, M. E., Derwent, R. G., Hayman, G. D., Alfarra, M. R., Coe, H., and McFiggans, G.: Simulating regional scale secondary organic aerosol formation during the TORCH 2003 campaign in the southern UK, Atmos. Chem. Phys., 6, 403–418, doi:10.5194/acp-6-403-2006, 2006. 21067
McFiggans, G., Topping, D. O., and Barley, M. H.: The sensitivity of secondary organic aerosol component partitioning to the predictions of component properties – Part 1: A systematic evaluation of some available estimation techniques, Atmos. Chem. Phys., 10, 10255–10272, doi:10.5194/acp-10-10255-2010, 2010. 21057, 21058, 21060, 21062, 21065, 21067, 21069, 21073
Myrdal, P. B. and Yalkowsky, S. H.: Estimating pure component vapor pressures of complex organic molecules, Industrial and Engineering Chemistry Research, 36, 2494–2499, 1997. 21060
Nannoolal, Y., Rarey, J., Ramjugernath, D., and Cordes, W.: Estimation of pure component properties Part 1. Estimation of the normal boiling point of non-electrolyte organic compounds via group contributions and group interactions, Fluid Phase Equilibria, 226, 45–63,

ACPD
11, 21055–21090, 2011

2004. 21060
Nannoolal, Y., Rarey, J., and Ramjugernath, D.: Estimation of pure component properties. Part 3. Estimation of the vapor pressure of non-electrolyte organic compounds via group contributions and group interactions, Fluid Phase Equilibria, 269, 117–133, 2008. 21060
Pankow, J. F.: An Absorption Model of Gas-Particle Partitioning of Organic Compounds in the Atmosphere, Atmos. Environ., 28, 185–188, 1994. 21061
Peng, C., Chan, M. N., and Chan, C. K.: The Hygroscopic Properties of Dicarboxylic and Multifunctional Acids : Measurements and UNIFAC Predictions, Environ. Sci. Technol., 35, 4495–4501, doi:10.1021/es0107531, 2001. 21061
Reemtsma, T., These, A., Venkatachari, P., Xia, X. Y., Hopke, P. K., Springer, A., and Linscheid, M.: Identification of fulvic acids and sulfated and nitrated analogues in atmospheric aerosol by electrospray ionization Fourier transform ion cyclotron resonance mass spectrometry, Anal. Chem., 78, 8299–8304, 2006. 21060, 21070
Reinhardt, A., Emmenegger, C., Gerrits, B., Panse, C., Dommen, J., Baltensperger, U., Zenobi, R., and Kalberer, M.: Ultrahigh Mass Resolution and Accurate Mass Measurements as a Tool To Characterize Oligomers in Secondary Organic Aerosols, Anal. Chem., 79, 4074–4082, doi:10.1029/2005GL023831, 2007. 21070
Saunders, S. M., Jenkin, M. E., Derwent, R. G., and Pilling, M. J.: Protocol for the development of the Master Chemical Mechanism, MCM v3 (Part A): tropospheric degradation of non-aromatic volatile organic compounds, Atmos. Chem. Phys., 3, 161–180, doi:10.5194/acp-3-161-2003, 2003. 21056
Stein, S. E. and Brown, R. L.: Estimation of Normal Boiling Points from Group Contributions, Journal of Chemical Information and Computational Science, 34, 581–587, 1994. 21060
Sun, Y.-L., Zhang, Q., Schwab, J. J., Demerjian, K. L., Chen, W.-N., Bae, M.-S., Hung, H.-M., Hogrefe, O., Frank, B., Rattigan, O. V., and Lin, Y.-C.: Characterization of the sources and processes of organic and inorganic aerosols in New York city with a high-resolution time-of-flight aerosol mass apectrometer, Atmos. Chem. Phys., 11, 1581–1602, doi:10.5194/acp-11-1581-2011, 2011. 21070, 21071
Topping, D. O., Barley, M. H., and McFiggans, G.: The sensitivity of Secondary Organic Aerosol component partitioning to the predictions of component properties: part 2; determination of particle hygroscopicity and its dependence on “apparent” volatility, Atmos. Chem. Phys. Discuss., 11, 9019–9056, doi:10.5194/acpd-11-9019-2011, 2011. 21057, 21060, 21065
Valorso, R., Aumont, B., Camredon, M., Raventos-Duran, T., Mouchel-Vallon, C., Ng, N. L.,

ACPD
11, 21055–21090, 2011

Seinfeld, J. H., Lee-Taylor, J., and Madronich, S.: Explicit modelling of SOA formation from α-pinene photooxidation: sensitivity to vapour pressure estimation, Atmos. Chem. Phys., 11, 6895–6910, doi:10.5194/acp-11-6895-2011, 2011. 21066, 21070

Zuend, A., Marcolli, C., Booth, A. M., Lienhard, D. M., Soonsin, V., Krieger, U. K., Topping, D. O., McFiggans, G., Peter, T., and Seinfeld, J. H.: New and extended parameterization of the thermodynamic model AIOMFAC: calculation of activity coefficients for organic-inorganic mixtures containing carboxyl, hydroxyl, carbonyl, ether, ester, alkenyl, alkyl, and aromatic functional groups, Atmos. Chem. Phys. Discuss., 11, 15297–15416, doi:10.5194/acpd-11-15297-2011, 2011. 21072

ACPD

11, 21055–21090, 2011

Table 1. Conditions for the partitioning calculations used with each scenario (all combinations used giving 32 cases).

Temperature (K)	Relative Humidity %	Involatile core $\mu g\, m^{-3}$
273.15	10	0.5
283.15	30	3.0
293.15	70	
303.15	80	

ACPD
11, 21055–21090, 2011

Table 2. Combinations of (p^0) and (γ_i) predictive techniques used within absorptive partitioning calculations .

p^0"VP" method	p^0"Tb" method	(γ_i) method	reference	notes
Nannoolal	Nannoolal	ideal ($\gamma_i = 1$)	N-N/VP	"base case"
Nannoolal	Stein and Brown	ideal ($\gamma_i = 1$)	SB-N/VP	
Nannoolal	Joback	ideal ($\gamma_i = 1$)	JR-N/VP	
Myrdal and Yalkowsky	Nannoolal	ideal ($\gamma_i = 1$)	N-MY	
Myrdal and Yalkowsky	Stein and Brown	ideal ($\gamma_i = 1$)	SB-MY	
Myrdal and Yalkowsky	Joback	ideal ($\gamma_i = 1$)	JR-MY	
Nannoolal	Nannoolal	non-ideal ($\gamma_i \neq 1$)	N-N/VP act	

ACPD
11, 21055–21090, 2011

Table 3. Some statistics for the variation in factor difference in SOA mass with (p^0) and (γ_i) models compared to the base case – see Fig. 2.

Model	Median	Mean	Std. Dev. (σ)	RSD = σ/Mean
SB-N/VP	1.09	1.19	0.31	0.26
JR-N/VP	17.78	39.87	82.46	2.07
N-MY	0.11	0.13	0.08	0.63
SB-MY	0.16	0.19	0.13	0.69
JR-MY	6.45	14.89	31.80	2.14
Hyd	2.04	3.68	5.74	1.56
N-N/VP act	0.97	0.97	0.62	0.63

ACPD
11, 21055–21090, 2011

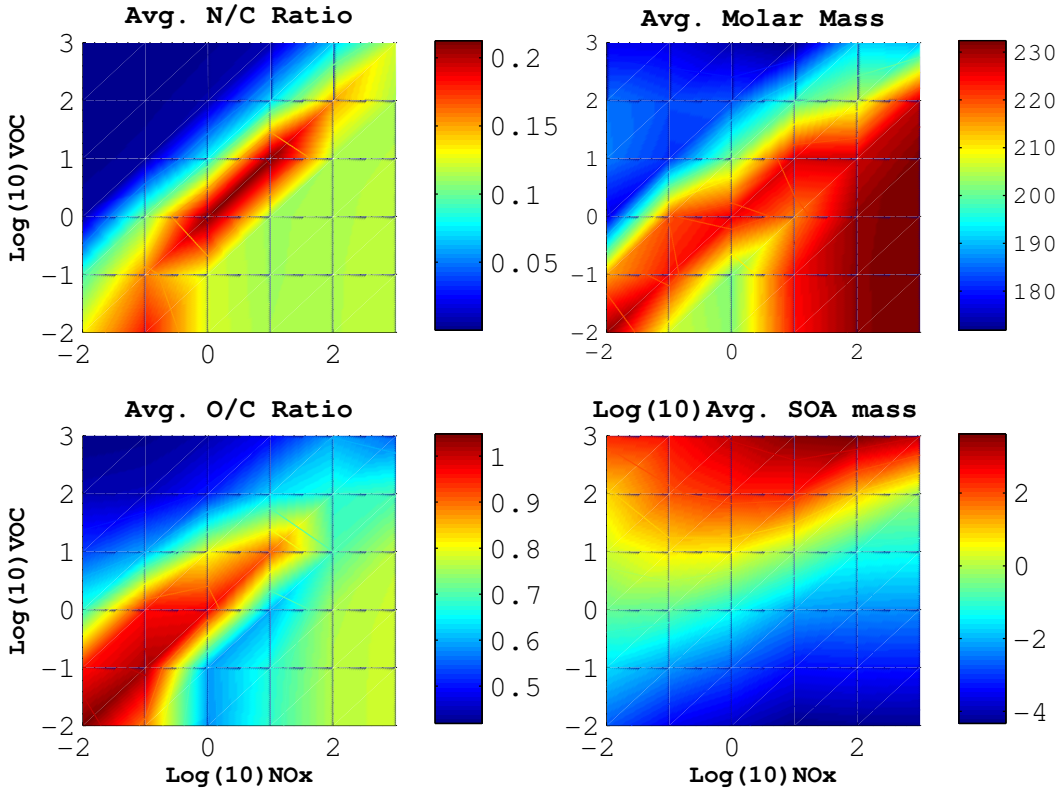

Fig. 1. Surface plots of key properties for those scenarios with AVOC = BVOC; the $\log_{10}$ AVOC being plotted on the y axis and $\log_{10}$ NO_x along the x axis in all 4 subplots; all at conditions $T = 293.15$ K, % RH = 70 and 3.0 µg m^{-3} involatile core. SOA mass is in µg m^{-3}.

ACPD
11, 21055–21090, 2011

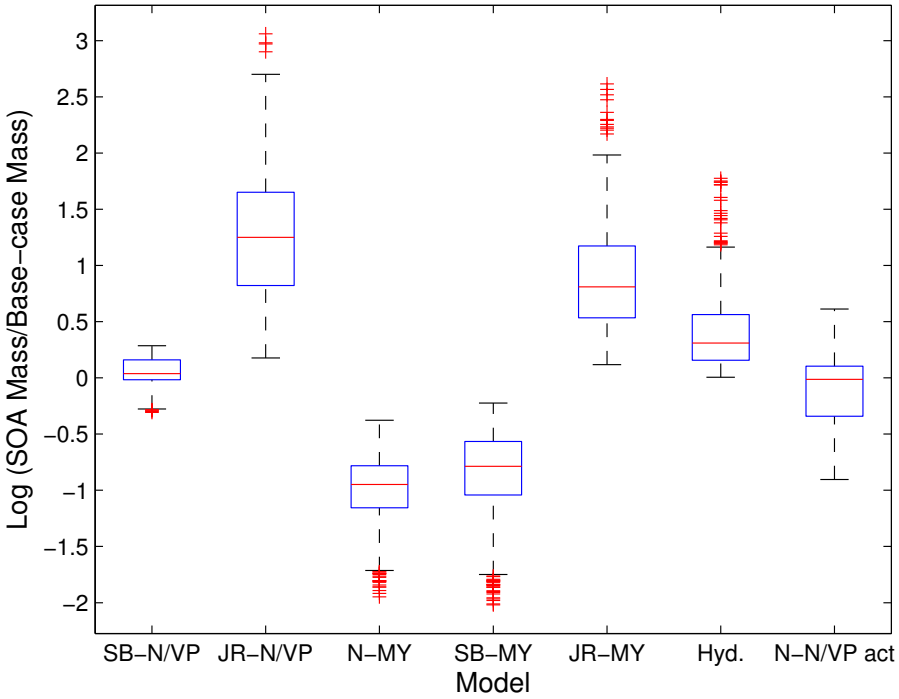

Fig. 2. Box-whisker plots showing the sensitivities of the predicted SOA mass, compared to the base case, across all cases for 27 scenarios using the partitioning model with **(a)** five vapour pressure estimation methods (plots 1–5, 2742 compounds, $\gamma_i = 1$); **(b)** plot 6 shows the effect of hydrolysis of acid anhydrides (2727 MCM compounds, p^0 by N/N-VP, $\gamma_i = 1$); **(c)** plot 7 shows the sensitivity to non-ideality (2742 compounds, p^0 by N/N-VP, γ_i by UNIFAC).

ACPD
11, 21055–21090, 2011

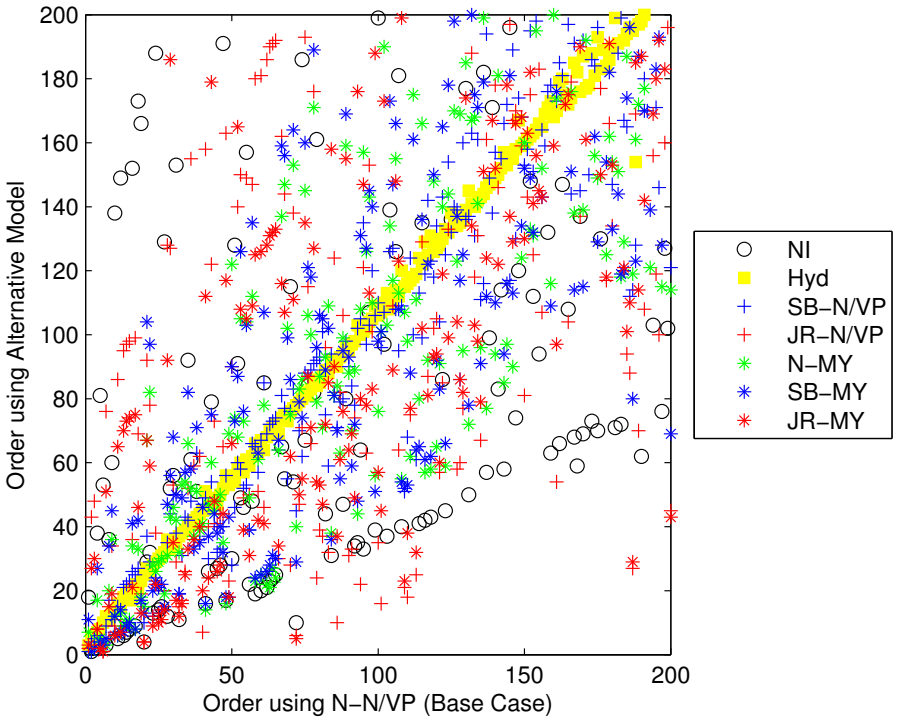

Fig. 3. Scatter plots showing the changes in the order of the top 200 compounds contributing to predicted SOA mass, compared to the base case (X-axis). SOA compositions used were from the standard (1.0/1.0/1.0) scenario; with $T = 293.15$ K, % RH = 70 and 3.0 µg m^{-3} involatile core. NI = N-N/VP act.

ACPD
11, 21055–21090, 2011

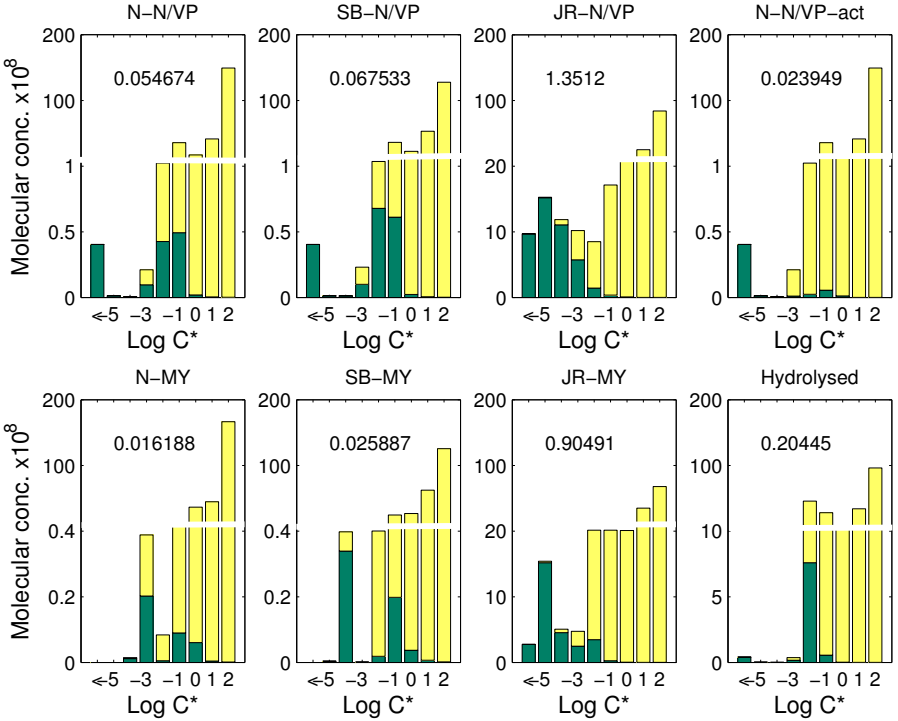

Fig. 4. Predicted binned component volatility for 2742 MCM compounds (except panel 8: 2727 compounds) with concentrations taken from the standard scenario (1.0/1.0/1.0 NO_x/AVOC/BVOC) with $T = 293.15$ K, % RH = 70 and 3.0 µg m^{-3}involatile core. The abscissa is the base 10 logarithm of the saturation concentration of the components in the respective volatility bin, while the y-axis gives the cumulative molecular concentration (in molecules cm^{-3}) for each bin: note scale change. The green bars correspond to the particulate and the yellow to the vapour phase. The total condensed SOA mass (in µg m^{-3}) is indicated on each panel.

ACPD
11, 21055–21090, 2011

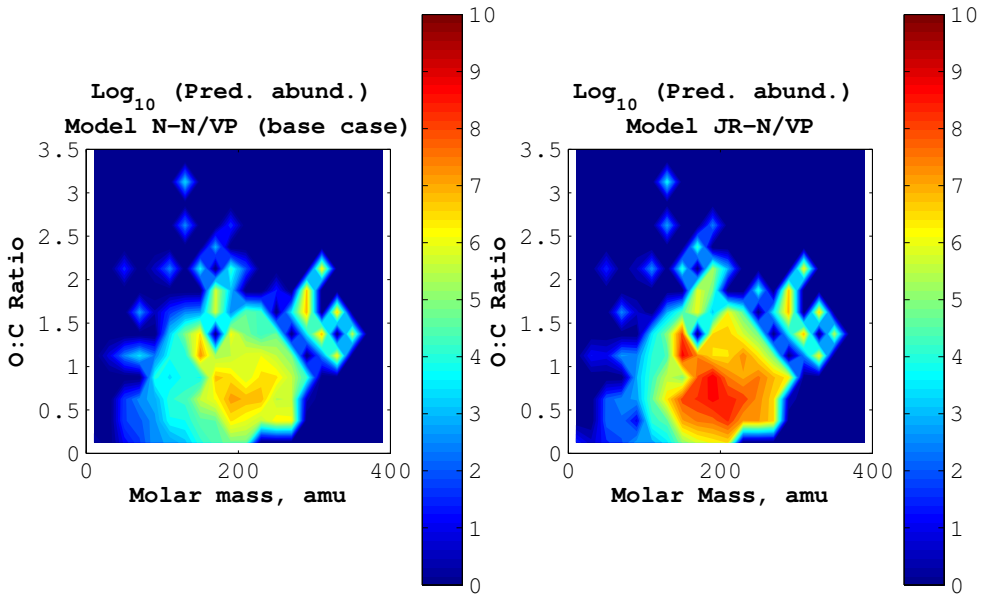

Fig. 5. Predicted binned organic component condensed moles plotted as a function of molar mass and O:C ratio for the 2742 MCM compounds with concentrations taken from the standard scenario (1.0/1.0/1.0 NO_x/AVOC/BVOC) with T = 293.15 K, % RH = 70 and 3.0 µg m^{-3}involatile core. The colour axis is the base 10 logarithm of the cumulative concentration of the condensed components (in molecules cm^{-3}) in the respective bin. The bins are defined by a subdivision of the O:C scale into bin width of 0.25, and the MW scale into bin widths of 20 g $mole^{-1}$. The left hand panel shows the distribution for the predicted composition generated using the N-N/VP (base case) model while the right hand panel shows a similar plot for the JR-N/VP model.

ACPD
11, 21055–21090, 2011

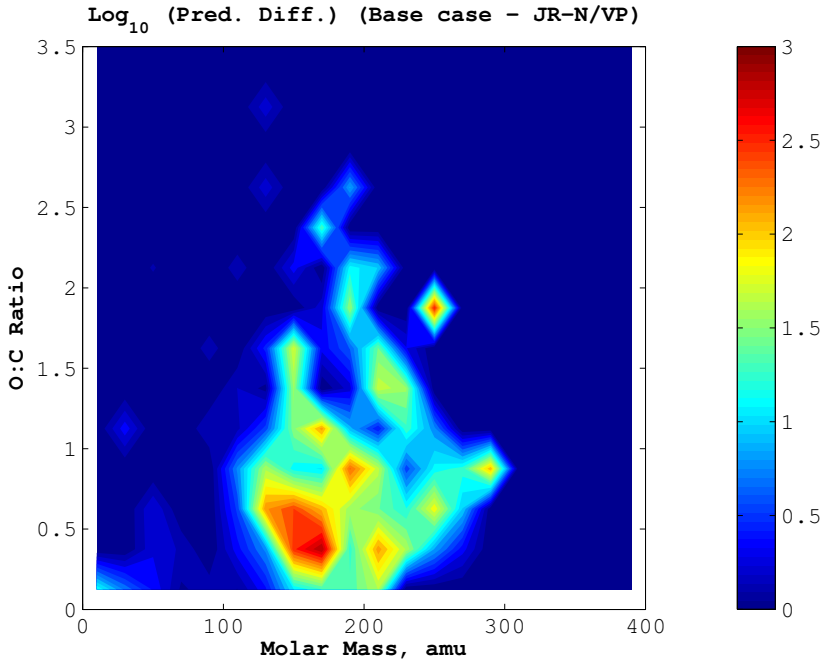

Fig. 6. The plot showing the factor difference in predicted binned organic condensed moles using the vapour pressure models shown in Fig. 5. The Z axis is the base 10 logarithm of the factor(JR-N/VP divided by N-N/VP) in the cumulative concentration of the condensed components (in molecules cm^{-3}) with negative values given a value of zero on this scale.

ACPD
11, 21055–21090, 2011

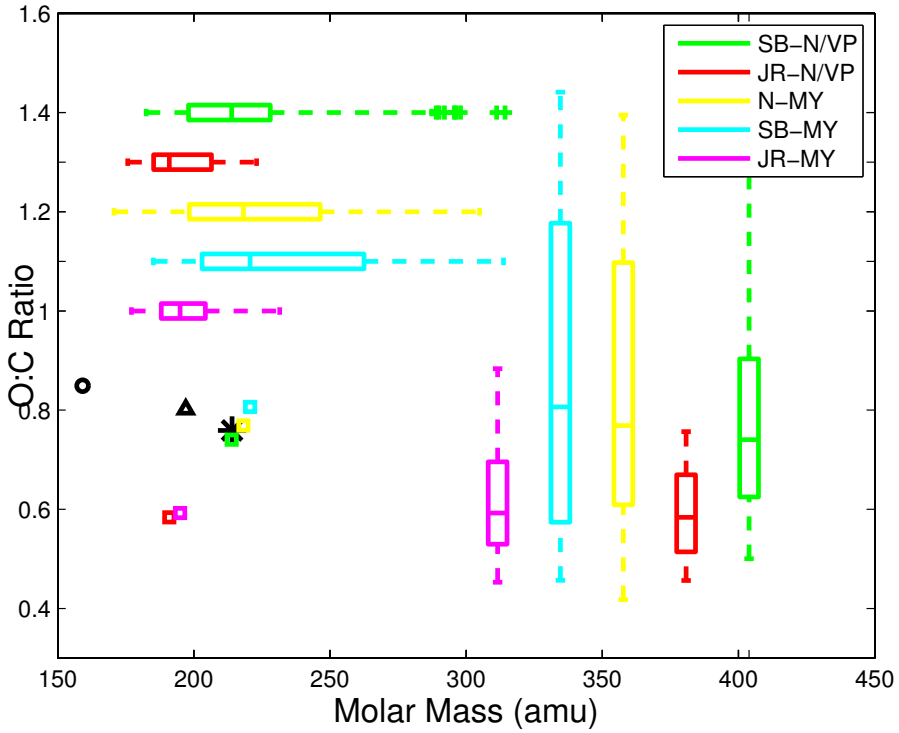

Fig. 7. The distribution of the average O:C ratios and molar masses of the predicted condensed SOA across all cases for 27 scenarios with the box-and-whiskers showing the median, interquartile and 95 % ranges for each combination of estimation techniques ($\gamma_i = 1$ assumed in all cases); the coloured squares show the median values for the corresponding box-whisker plots. The black symbols refer to the base-case and variants using the N-N/VP method: black asterisk- base case (p^0 by N-N/VP); black circle- hydrolysed case (2727 compounds, p^0 by N/N-VP); black triangle- non-ideal case (p^0 by N/N-VP, γ_i by UNIFAC).

ACPD
11, 21055–21090, 2011

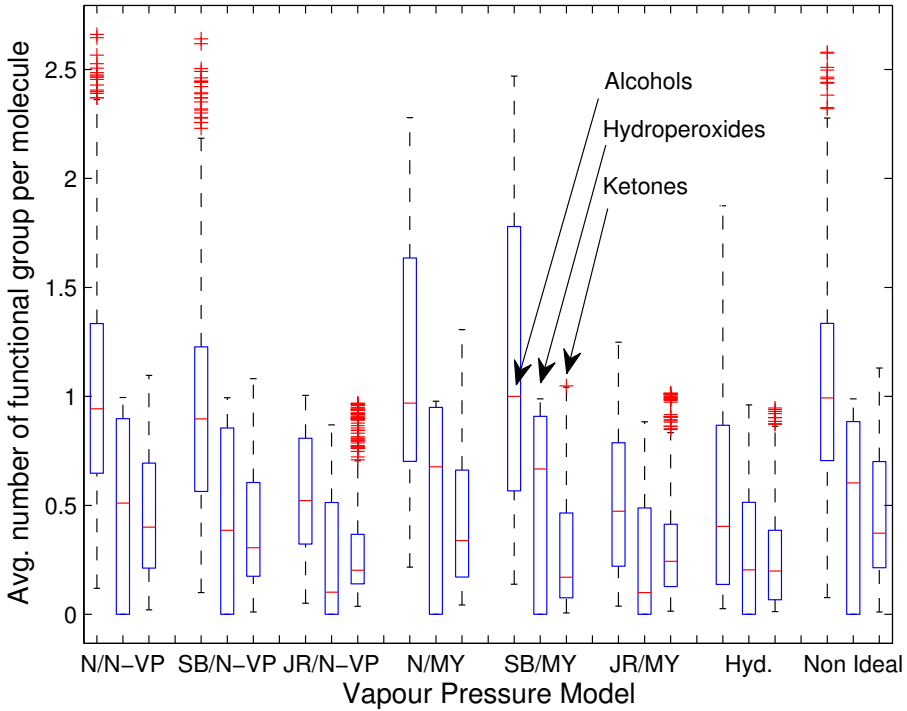

Fig. 8. Box-whisker plots showing the sensitivities of the average number of the three most abundant functional groups (alcohols, hydroperoxides and ketones) per molecule, across all cases for 27 scenarios using the partitioning model with **(a)** five vapour pressure estimation methods (plots 1–5, 2742 compounds, $\gamma_i = 1$); **(b)** plot 6 shows the effect of hydrolysis of acid anhydrides (2727 MCM compounds, p^0 by N/N-VP, $\gamma_i = 1$); **(c)** plot 7 shows the sensitivity to non-ideality (2742 compounds, p^0 by N/N-VP, γ_i by UNIFAC).

ACPD
11, 21055–21090, 2011

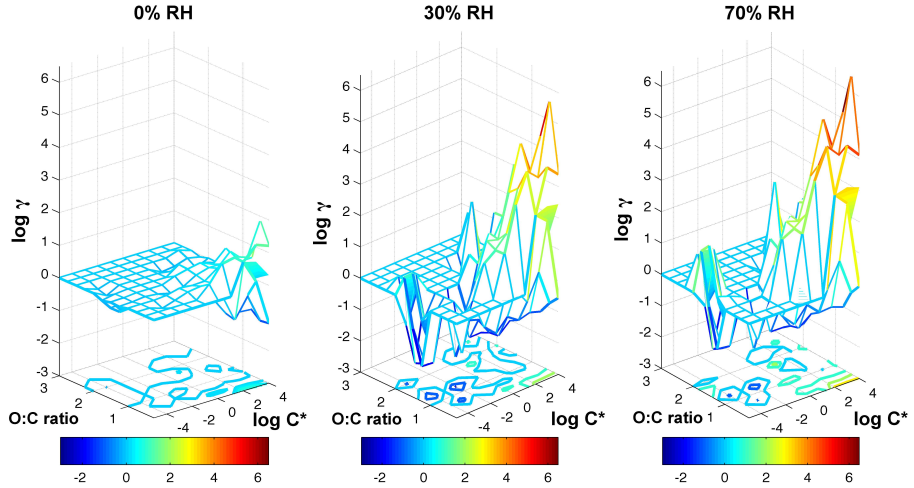

Fig. 9. Surface plots of $\log_{10}(\gamma_i)$ for the non-ideal calculation (2742 compounds, p^0 by N/N-VP, γ_i by UNIFAC) using the standard scenario (1.0/1.0/1.0 NO_x/AVOC/BVOC) under conditions $T = 293.15\,K$; $\%\,RH = 0$, 30 or 70; and $0.5\,\mu g\,m^{-3}$ involatile core. The two meshes show the minimum and maximum activity coefficients as a function of O:C ratio and $\log_{10}(C^*)$. The contour plot on the base of the figure shows the median value for each bin.

ACPD
11, 21055–21090, 2011